# GBM Modeling with Proliferation and Migration Phenotypes: A Proposal of Initialization for Real Cases

Juan Ortiz-Pla(✉), Elies Fuster-Garcia, Javier Juan-Albarracin, and Juan Miguel Garcia-Gomez

Instituto Universitario de Aplicaciones de las Tecnologias de la Informacion y de las Comunicaciones, Universidad Politecnica de Valencia, Camino de Vera s/n, 46022 Valencia, Spain
juaorpl@etsii.upv.es

**Abstract.** Glioblastoma is the most aggressive tumor originated in the central nervous system. Modeling its evolution is of great interest for therapy planning and early response to treatment assessment. Using a continuous multi-scale growth model, which considers the angiogenic process, oxygen supply and different phenotype expressions, a new method is proposed for setting the initial values of the celular variables, based on a spatiotemporal characterization of their distribution in controlled synthetic simulations. The method is applied to a real case showing an improvement on the dynamic stability, compared to the usual method.

**Keywords:** Glioblastoma growth · Mathematical model · Phenotype expression · *in silico* oncology

## 1 Introduction

Glioblastoma (GBM), also known as grade IV astrocytoma, is a brain neoplasm involving glial cells. It represents around 12–15% of all intracranial tumors and 50–60% of all astrocytomas. The survival mean time is 14 months, and the standar treatment involves surgery, chemotherapy and radiotherapy [1]. They share a common morphology: presence of brain edema, irregular borders, and a tumor ring surrounding a necrotic center [2].

Most of the works about tumor growth, deal with gliomas instead of GBM [3–5]. However, because GBM is a high grade glioma, many aspects and considerations of modeling proposed by these works are still valid when focusing only in GBM. Also, many authors agree in the important role that phenotype expressions, characterized as different cellular populations, play in the tumor growth dynamics [3–7]. The 'go-or-grow' hypothesis is widely extended and accepted for modeling. It states that phenotype expressions can be simplified into two groups: enhanced proliferation when the environment is favorable, and enhanced mobility


S.A. Tsaftaris et al. (Eds.): SASHIMI 2016, LNCS 9968, pp. 65–74, 2016.
DOI: 10.1007/978-3-319-46630-9_7

when the local availability of resources is low [8]. To model the local availability of resources in the tumor microenvironment, many studies have focused on modeling the angiogenesis cascade [3–5,9]. Although results are promising, the objective of these studies usually consists on replicating the branching and morphology of capillaries, rather than studying their effect on the growth dynamics. Recent articles of GBM growth include simplified versions of angiogenesis models to better characterize the supply of nutrients and its effect on phenotype change [6,7,10,11].

However, a common limitation to many of the mentioned works, is the lack of justification and methodology for the initialization of the variables of the model. This is due to the difficulty of establishing a relationship between the considered variables and the accessible clinical information for a patient. Even though anatomical images allow to segment the extension of the tumor, the information provided is typically a binary mask without quantifiable information about tumor cells or angiogenic variables. This problem becomes much more troublesome when different phenotype expressions, modeled as cellular populations, cohabit in the same segmented region.

In this work we use a continuous multi-scale GBM growth model, which considers the key physiological aspects of tumor progression: angiogenesis, oxygen supply and oxygen-mediated phenotype switch. Using this model we propose a methodology to initialize the values of the celular variables based on the characterization of their spatiotemporal distribution. We consider the hypothesis that, in a controlled homogeneous environment, after a certain time, the modeled physiological processes stabilize, and as a result, the spatial distributions of the different phenotypes across the tumor reach a stationary morphology. Our proposed method uses this knowledge in real cases, to assign an initial value to the variables for each point of the anatomical segmentation.

## 2 Materials and Methods

### 2.1 GBM Growth Model

We propose a set of spatiotemporal, coupled, non-linear partial derivative equations (PDE), which represent the most relevant features of the GBM's growth dynamics:

$$\frac{\partial g}{\partial t} = \bigtriangledown \cdot (D_g \bigtriangledown g) + \rho_g\ g\ (1 - T) + (\theta_{mg}\ H_{mg})\ m - (\theta_{gm}\ H_{gm})\ g \tag{1}$$

$$\frac{\partial m}{\partial t} = \bigtriangledown \cdot (D_m \bigtriangledown m) + \rho_m\ m\ (1 - T) + (\theta_{gm}\ H_{gm})\ g - (\theta_{mg}\ H_{mg})\ m - (\theta_{mN} H_{mN}) m \tag{2}$$

$$\frac{\partial N}{\partial t} = (\theta_{mN} H_{mN}) m + (\theta_{vN} H_{vN}) v \tag{3}$$

$$\frac{\partial o}{\partial t} = (1 - o)\varphi\ v - o\Big(\frac{\alpha_g g + \alpha_m m}{K_m + o}\Big) \tag{4}$$

$$\frac{\partial a}{\partial t} = \bigtriangledown \cdot (D_a \bigtriangledown a) + \rho_{am}\ m - \gamma\ v \tag{5}$$

$$\frac{\partial v}{\partial t} = \bigtriangledown \cdot (\chi v \bigtriangledown a) + \rho_v\ v\ m\ (1 - N) - (\theta_{vN} H_{vN}) v \tag{6}$$

Where $g$ is the density of proliferative cells, $m$ is the density of invasive cells, $N$ is the necrosis area of the tumor, $o$ is the oxygen concentration, $v$ is the density of vascularization and $a$ is the concentration of angiogenic factors. $T$ is the total tumor density, which is $T = g + m + N$. All variables are normalized by their maximum possible value, and as a result they all $\in [0, 1]$. A complete list and explanation of the parameters can be found in Table 1.

The basic assumptions of this model are:

- Cells diffuse through the extracellular matrix (ECM) with brownian movement. We assume that invasive cells $m$ are more able to move than proliferative cells $g$, and thus we impose $D_m > D_g$.
- Cellular proliferation follows a logistic law. The total tumoral density $T$ shall not grow over the maximum carrying capacity of the tissue $K_{max}$.
- Based on the modeling hypothesis *'go-or-grow'* we consider two different phenotype expressions, separated into different cell populations: proliferative cells $g$ and invasive cells $m$. The change from one population to another is mediated by the local availability of oxygen. We establish a hypoxia threshold $O_{2hyp}$ and we define the functions $H_{mg}$ and $H_{gm}$ as step functions such as:

$$H_{mg} = \begin{cases} 1, & \text{if } o > O_{2hyp} \\ 0, & \text{otherwise} \end{cases} \tag{7}$$

$$H_{gm} = 1 - H_{mg} \tag{8}$$

- When hypoxia is too severe, cells die by necrosis. We set the severe hypoxia threshold to $O_{2death}$ and, in the same way as before, we define the step functions $H_{mN}$ and $H_{vN}$ as:

$$H_{mN} = H_{vN} = \begin{cases} 1, & \text{if } o < O_{2death} \\ 0, & \text{otherwise} \end{cases} \tag{9}$$

- Oxygen consumption by cancer cells can be modeled in Eq. (4) using the Michaelis-Menten law for enzyme kinetics. This law corresponds to an asymptotic curve, implying that no matter how much oxygen available there might be, there is a maximum rate of consumption achievable.
- Oxygen supply from the capillaries to the ECM depends on the permeability of the capillary wall, but mainly on the difference of partial pressure between the vase and the exterior. We can consider the partial pressure of oxygen in the capillaries $[O_2]_a$, in Eq. (4), to be a constant parameter.
- Invasive cells $m$ produce angiogenic factors $a$, which attract endothelial cells $v$ by chemotaxis. As a consequence vascular density increases. To avoid introducing another non-linear term, we assume that the consumption of angiogenic factors by endothelial cells occurs at a constant rate $\gamma$. Chemotaxis is represented in Eq. (6) as a flux of $v$ following the gradient of $a$.

To solve the equations we use an implicit finite difference scheme based on *Backwards-Time-Centered-Space* (BCTS) and an iterative predictor-corrector algorithm that allow us to initially decouple the whole system into two coupled subsystems to simplify the treatment of the non-linearities. The BCTS method has first order convergence in time and second order convergence in space. Is generally stable, so it is possible to use wide time-steps.

### 2.2 Parameters of the Model

A common limitation to all tumor growth models is the huge amount of free parameters needed when coupling different effects. It is not feasible to devise mathematical methods to optimize and identify the whole set of parameters, and therefore the usual approach consists on identifying most values from the existing literature. We consider a division of the parameters of the model into two groups: patient-independent and patient-dependent. The patient-dependent are the parameters which deal directly with the tumor cells and the physical properties of the GBM. That is its invasive capability, given by the diffusivity parameters, its proliferation rate, and the agility to switch from one phenotype to another. These characteristics may vary between patients. The patient-independent parameters on the other hand, deal with the rest of the physiological processes modeled, and is reasonable to assume that are quite less variable and more constant through patients (Table 1).

In order to evaluate the impact of variating the patient-dependent parameters, we conduct a parametric sweep with relative increments and decrements of 50 % and 20 % over the reference value. The effect of these variations on the outcome result is analyzed by measuring the temporal evolution of the tumor mass, the tumor area and the tumor density.

### 2.3 Reference Synthetic Case

This case consists on a free growth simulation of a tumor spheroid of 0.2 cm of radius for 20 days in a $15 \times 15\,\mathrm{cm}^2$ grid of homogeneous white matter. The spatial step was set to $\Delta x = 0.1\,\mathrm{cm}$ and the time-step to $\Delta t = 0.05\ days$. The initial spheroid is composed only by proliferative cells with $g_0 = 1/3 \cdot K_{max}$ representing this way its young age and its growing phase. The initial oxygen concentration is set constant for the whole grid. Because the brain is an organ with a high oxygen consumption rate, we set the initial concentration to 60 % of its maximum partial pressure. The density of vascularization is also initialized as constant throughout the grid with $v_0 = 0.09 \cdot K_{max}$. Because initially there are no invasive cells $m$, the initial concentration for $a$ is zero.

### 2.4 Characterization of the Temporal Evolution of Cell Distributions

To validate our hypothesis of stabilization of the physiological processes that leads to stationary distributions of cellular populations, we propose a methodology in which we compare the statistical distances between such distributions

**Table 1.** List of parameters of the model

| **Patient-dependent parameters** | | | |
|---|---|---|---|
| Parameter | Value | Description | Reference |
| $D_g$ | $3.6 \cdot 10^{-8}$ cm$^2$/s | Diffusivity of $g$ | [10] |
| $D_m$ | $D_g/10$ | Diffusivity of $m$ | |
| $\rho_g$ | 1.8 $days^{-1}$ | Proliferation rate of $g$ | |
| $\rho_m$ | $\rho_g/2$ | Proliferation rate of $m$ | |
| $\theta_{gm}$ | 1 $days^{-1}$ | Rate of change $g$ to $m$ | |
| $\theta_{mg}$ | 1/3 $days^{-1}$ | Rate of change $m$ to $g$ | [12] |
| **Patient-independent parameters** | | | |
| Parameter | Value | Description | Reference |
| $D_a$ | $1.0 \cdot 10^{-5}$ cm$^2$/s | Diffusivity of $a$ | |
| $\rho_{am}$ | $1.0 \cdot 10^{-9}$ mol/s | Production of $a$ | |
| $\rho_v$ | $\rho_g/10$ | Proliferation rate of $v$ | |
| $\theta_{mN}$ | 1.2 $days^{-1}$ | Rate of death of $m$ | |
| $\theta_{vN}$ | $\theta_{mN}/10$ | Rate of death of $v$ | |
| $O_{2hyp}$ | 7 mmHg | Hypoxia threshold | [13] |
| $O_{2death}$ | 0.7 mmHg | Severe hypoxia threshold | [14] |
| $[O_2]_a$ | 60 mmHg | Arterial partial pressure of $o$ | [15] |
| $\alpha_g$ | $1.0 \cdot 10^{-17}$ mol/cell $\cdot$ s | Rate of consumption of $o$ by $g$ | [16] |
| $\alpha_m$ | $\alpha_g/5$ | Rate of consumption of $o$ by $m$ | [16] |
| $\gamma$ | $\alpha_g$ | Rate of consumption of $a$ by $v$ | |
| $\varphi$ | 0.3 | Vascular supply parameter | |
| $\chi$ | 0.1 | Chemotaxis mobility parameter | [9] |
| $K_{max}$ | $1.0 \cdot 10^6$ cell/cm$^2$ | Maximum carrying capacity of cells | [17] |

at different stages of the evolution of GBM growth, using simulations based on the reference synthetic case.

We will use the Jensen-Shannon divergence (JS) to compare the similarities of the distributions of $m$ and $g$ in each time-step against the distribution of the last time-step. In order to do that we need to convert the curves to statistical distributions and align them at the point of their maximal cross-correlation, as we are only interested in comparing their morphology.

### 2.5 Initialization of $g$ and $m$ Cell Distributions for a Real Case

Our main objective in this study is to be able to initialize the variables of the model in a real case tumor based on information of magnetic resonance images (MRI). A correct estimation of the initial values of the variables is of the utmost

importance for the success of the simulation and, therefore, for increasing the predictive capability of the model.

In MRI there is not a direct correspondence between the intensity of the voxel and tumor density. Some studies observed that the detection threshold for GBM in a T1-weighted image (T1) is much greater than that of a T2-weighted image [18]. Because active tumor segmentation masks are based mainly on T1, it is safe to assume that there is tumoral tissue outside the segmented area.

In simple models in which there is only one type of cellular population, the usual method of initialization is to consider the whole segmented ring to be saturated at the carrying capacity and smooth it with a gaussian filter. The same approach is used when two cellular populations are considered. However, to assume an homogenous distribution of both variables across the segmented ring, is too simple. Based on our hypothesis of the stabilization of the distributions over time in controlled homogeneous cases, we propose a methodology for real cases in which we assign a different density value to each point, depending on their relative position inside the active tumor. We will compare our methodology to the usual initialization method previously described.

Considering we have a distribution curve for $g$ and $m$, we take into account the threshold of detection of GBM for T1 in order to define the active tumor region from these distribution curves. This threshold value is not given in the literature as it is not possible to estimate accurately, but we can consider it to be greater than 50 % of the maximum density based on the existing graphic representations in the literature [18]. We then normalize the distributions for the width of $(g + m)$ that should be detected by the mentioned threshold, resulting in $x = 0$ for the inner border and $x = 1$ for the outer border as can be seen in Fig. 1, with $x$ being the relative spatial position.

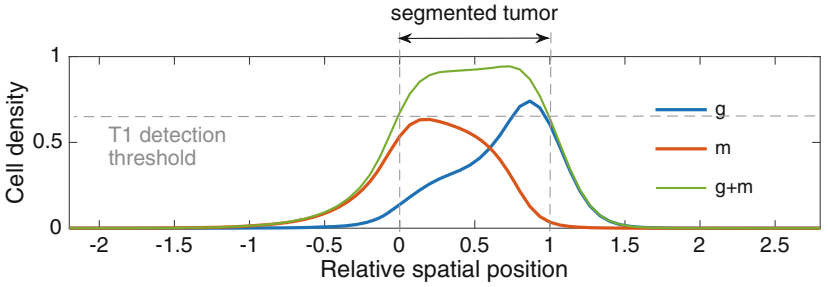


**Fig. 1.** Example of normalized distribution of $g$ and $m$ by the width given by the T1 detection threshold

In order to apply these distribution functions to a real case we differentiate between points belonging to the binary mask, points enclosed by the binary mask and points outside of the binary mask. In the first case we compute the geodesic distance of each point to the inner and outer boundary. We assume that the sum of those values is a good estimator of the width. Dividing the distance to the

inner border by the estimated width, we obtain the relative position inside the segmentation. For the points enclosed by the mask we only need the geodesic distance to the inner boundary, and similarly, for the exterior points, only the distance to the outer boundary is needed. Those values are then used to get the corresponding density value from the distribution curves $g$ and $m$.

To test the proposed method we used GBM data from the MICCAI BRATS Challenge 2013 training set. A detailed explanation of the method and parameters of acquisition of the data set can be found in [19].

## 3 Results

### 3.1 Variation of Parameters

**Variation of Diffusivity ($D_g$).** When varying the diffusivity of cells, a direct relationship is observed with the tumor mass and the tumor area: both variables increase when diffusivity increases, and decrease when diffusivity decreases. The density increases as the diffusivity decreases, which seems logical, but also increases when diffusivity increases. This may seem counterintuitive at first, however it can be explained by the fact that with higher mobility, tumor cells might be able to access better oxygenated areas and sustain a proliferative profile for a longer period of time.

**Variation of Proliferation Rate ($\rho$).** There is a direct relationship between the parameter and all the measured variables. It is noticeable that our model is very sensible to variations in this parameter: the relative variation of the outcome is greater than the relative variation of the parameter value.

**Variation of Phenotype Change Rates ($\theta_{gm}, \theta_{mg}$).** The variation of theses parameters has a minimum impact on the outcome of the simulations. Relative mass and area variations are consistently under 10 %, and density stays under 1 %.

### 3.2 Characterization of the Temporal Evolution of Cell Distributions

In Fig. 2a, we obtain a curve showing that the JS distance between each distribution and the last one, convergences to zero. That means that from a certain time-step onwards, the distribution of both cellular populations across the ring, reaches a constant shape. That shape is represented in Fig. 2b.

### 3.3 Initialization of a Real Case

Having demonstrated that our model reaches stationary distributions for $g$ and $m$, we apply our initialization to a real tumor based on the segmentation of its

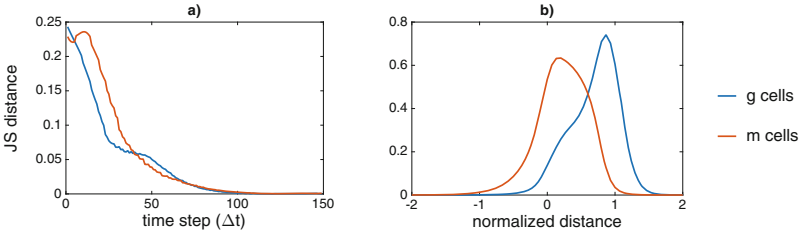


**Fig. 2.** (a) Convergence of the JS distance between distributions of $g$ and $m$ over time. (b) Stationary distribution of $g$ and $m$ for the reference case.

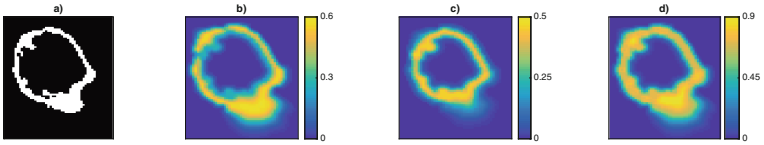


**Fig. 3.** (a) Segmentation mask. (b) Estimated density of $g$. (c) Estimated density of $m$. (d) Total estimated density $g + m$

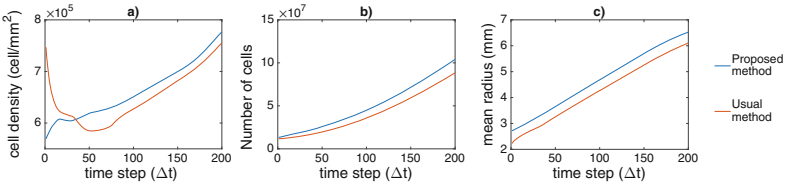


**Fig. 4.** Comparison between our proposed initialization method and the previous one. (a) Evolution of tumor density over time. (b) Number of cells over time. (c) Mean radius over time.

active tumor ring (Fig. 3a). The enclosed area inside corresponds to necrosis, and the peripheral edema is not represented. Figures 3b and c show the initial distribution of each phenotype according to our method, and Fig. 3d represents the total active tumor $g + m$.

Figure 4 compares the evolution of tumor density, number of cells and mean radius over time between our proposed method and the current one. Although both need some stabilization time at the beginning (Fig. 4a), it is much shorter for our methodology and the inertia of growth is better kept. The usual method needs to go through a transitory phase to reach the steady-state growth, and as a consequence it lags behind and initially loses the growth inertia.

## 4 Discussion

In this study we have proposed a new multi-scale GBM growth model which considers the angiogenic cascade, oxygen supply and its effect on the cellular

population. The mathematical complexity is a problem, and as a consequence, a huge number of free parameters are needed. Most of these parameters could be assumed to be patient-independent which could be defined from the existing literature, and select just a small group to estimate for each patient. In this sense, our parametric study serves two purposes: first, we assess how the model responds to variations of the selected parameters, to identify those with the highest impact on the outcome. Then, with our sight set on evaluating real cases, we personalize the estimation of the most relevant parameters to each patient.

Our parametric sweep concluded that cellular diffusivity and proliferation rates are the most relevant of the patient-dependent parameters in terms of total mass, invaded area and density. Those results are consistent with the wave-front propagation speed of the Fisher-Kolmogorov equation ($v = 2\sqrt{\rho D}$). Due to the different formulation of our equations, our model is more sensible to $\rho$ than to $D$, although both play a central role.

We have successfully demonstrated, using the JS divergence, that in an homogeneous controlled grid, after enough time-steps, our model yields a constant distribution of $g$ and $m$ along the tumor ring. Using this knowledge, we devised a method to successfully initialize a real tumor based on a binary segmentation and showed a dynamic improvement over the usual method. We consider this to be a good advance towards a more precise and more informed initialization of the variables in real cases, as we are able to assign density values to nodes beyond the binary mask. However, the current limitations of our method are: first the assumption of stationary growth state at the acquisition time, and second, it only has physiological sense for tumors with an enclosed necrotic center. There is need for more validation with longitudinal cases, comparing time points, and further characterization of the distributions, taking into account inhomogeneities that may be found on real brains.

## 5 Conclusion

We have demonstrated that our controlled reference simulation arrives, after certain time-steps, to a stationary growth state in which the distributions of $g$ and $m$ remain constant in shape across the tumor ring. Using this knowledge we have successfully initialized a real tumor from a binary segmentation mask. Our methodology for initializing the variables of the tumor is both informed and realistic, as it indicates the presence of cancer cells beyond the binary mask. It also shows an improvement in the dynamic performance of the model, compared to the usual method, as it takes less time-steps to stabilize and reach a stationary growth state.

**Acknowledgments.** This work was partially supported by Project TIN2013- 43457-R funded by the Ministerio de Economia y Competitividad of Spain, the GLIOMARKERS project funded by the INBIO joint action between UPV and IIS HUPLF, and the CURIAM-FDFT project funded by ITACA-UPV EMBLEMA action. E. Fuster-Garcia acknowledges the financial support from the UPV PAID-10–14 grant.

## References


1. Harter, D.H., et al.: Glioblastoma multiforme: state of the art and future therapeutics. Surg. Neurol. Int. **5**(1), 64 (2014)
2. Kumar, V., et al.: Robbins and Cotran Pathologic Basis of Disease. Elsevier Saunders, Philadelphia (2005)
3. Tang, L., et al.: Computational modeling of 3D tumor growth and angiogenesis for chemotherapy evaluation. PLoS ONE **9**(1), e83962 (2014)
4. Swanson, K.R., et al.: Quantifying the role of angiogenesis in malignant progression of gliomas: in silico modeling integrates imaging and histology. Cancer Res. **71**(24), 7366–7375 (2011)
5. Cai, Y., et al.: Coupled modelling of tumour angiogenesis, tumour growth and blood perfusion. J. Theor. Biol. **279**(1), 90–101 (2011)
6. Martnez-Gonzlez, A., et al.: Hypoxic cell waves around necrotic cores in glioblastoma: a biomathematical model and its therapeutic implications. Bull. Math. Biol. **74**(12), 2875–2896 (2012)
7. Saut, O., et al.: A multilayer grow-or-go model for gbm: effects of invasive cells and anti-angiogenesis on growth. Bull. Math. Biol. **76**(9), 2306–2333 (2014)
8. Gerlee, P., et al.: The impact of phenotypic switching on glioblastoma growth and invasion. PLoS Comput. Biol. **8**(6), e1002556 (2012)
9. Manoussaki, D.: A mechanochemical model of angiogenesis and vasculogenesis. ESAIM. Math. Model. Numer. Anal. **37**(04), 581–599 (2003)
10. Marias, K., et al.: A proposed paradigm shift in initializing cancer predictive models with dce-mri based pk parameters: a feasibility study. Cancer Inf. **14**(Suppl. 4), 7 (2015)
11. Eikenberry, S.E., et al.: Virtual glioblastoma: growth, migration and treatment in a three-dimensional mathematical model. Cell Prolif. **42**(4), 511–528 (2009)
12. Jewell, U.R.: Induction of HIF-1a in response to hypoxia is instantaneous. FASEB J. **15**(7), 1312–1314 (2001)
13. Vaupel, P.: The role of hypoxia-induced factors in tumor progression. Oncologist **9**(Suppl. 5), 10–17 (2004)
14. Martin Brown, J., et al.: Exploiting tumour hypoxia in cancer treatment. Nat. Rev. Cancer **4**(6), 437–447 (2004)
15. McLellan, S.A., et al.: Oxygen delivery and haemoglobin. Continuing Educ. Anaesth. Crit. Care Pain **4**(4), 123–126 (2004)
16. Grimes, D.R., et al.: A method for estimating the oxygen consumption rate in multicellular tumour spheroids. J. Roy. Soc. Interface **11**(92), 20131124 (2014)
17. Rockne, R., et al.: Predicting the efficacy of radiotherapy in individual glioblastoma patients in vivo: a mathematical modeling approach. Phys. Med. Biol. **55**(12), 3271–3285 (2010)
18. Harpold, H.L.P., et al.: The evolution of mathematical modeling of glioma proliferation and invasion. J. Neuropathol. Exp. Neurol. **66**(1), 1–9 (2007)
19. Menze, B.H., et al.: The multimodal brain tumor image segmentation benchmark (BRATS). IEEE Trans. Med. Imaging **34**(10), 1993–2024 (2015)